

Adiabatic spin-transfer-torque-induced domain wall creep in a magnetic metal

S. DuttaGupta¹, S. Fukami^{2,3}, C. Zhang¹, H. Sato^{2,3}, M. Yamanouchi^{1,2}, F. Matsukura^{1,2,4}
and H. Ohno^{1,2,3,4*}

The dynamics of elastic interfaces is a general field of interest in statistical physics, where magnetic domain wall has served as a prototypical example. Domain wall 'creep' under the action of sub-threshold driving forces with thermal activation is known to be described by a scaling law with a certain universality class¹⁻¹⁰, which represents the mechanism of the interaction of domain walls with the applied forces over the disorder of the system. Here we show different universality classes depending on the driving forces, magnetic field or spin-polarized current, in a metallic system, which have hitherto been seen only in a magnetic semiconductor^{3,6}. We reveal that an adiabatic spin-transfer torque plays a major role in determining the universality class of current-induced creep, which does not depend on the intricacies of material disorder. Our results shed light on the physics of the creep motion of domain walls and other elastic systems.

The creep motion of elastic interfaces in disordered media shares the same physics for a wide variety of objects, including vortex and/or domain walls (DWs) in superconductors, and ferromagnetic and ferroelectric systems, fluid wetting/propagation, the growth of bacterial colonies and so on¹¹⁻¹³. The creep velocity v obeys a universal Arrhenius scaling relation as $\log(v) \propto f^{-\mu}$, with a 'creep' exponent μ which defines the universality class of the motion¹⁴. A magnetic DW is an interface between two domains with different magnetization directions and its motion is induced by a magnetic field or spin-polarized current¹⁵⁻²⁴. Earlier studies on field-induced DW creep indicated that the motion is categorized into a universality class with random bond (RB) or random field (RF), which is characterized by $\mu = 0.25$ or 1, respectively¹⁻¹⁰, depending on the nature of disorder in the system. On the other hand, the universality class for current-induced motion is highly controversial. This is due to the fundamental difference between the interaction of a DW with current as compared to magnetic field; a magnetic field induces DW motion by lowering the Zeeman energy, whereas a current exerts various torques with different symmetries on the DW. Experiments on magnetic semiconductor and metallic systems revealed different scenarios. In the case of a magnetic semiconductor (Ga,Mn)As, whereas the field-induced DW creep falls into the RF or RB picture depending on the surface roughness, the current-driven creep belongs to a different universality class regardless of the nature of the disorder^{3,6}. On the other hand, in the case of magnetic metals both the field- and current-driven DW creep belong to the RB universality class characterized by $\mu = 0.25$ (ref. 7), suggesting that the current acts as an effective magnetic field. The field-like spin-transfer torque (STT) is known to be brought

about by a non-adiabatic STT related to the deviation of spin transport from the adiabatic condition or spin-orbit torque (SOT) recently found for systems with structural inversion asymmetry^{7,17}. However, no clear consensus has yet been achieved on the question of the universality class for adiabatic STT-induced DW creep in magnetic metals.

In this work, we focus on the unsolved issue of the universality class for current-induced DW creep in magnetic metals. Particularly, whether different universality classes between the field- and current-induced creeps is possible in magnetic metals deserves further attention. This will shed light on the question of what governs the universality class for the current-driven creep. To settle this issue, we employ a CoFeB/MgO metallic system²⁵ having a different nature of disorder as compared to the magnetic semiconductor³. Whereas the disorder originates most probably from the magnetic moments of randomly distributed impurity atoms in the ferromagnetic semiconductor, falling into the long-ranged RF model, that in CoFeB/MgO system is expected to originate from local defects such as surface roughness, falling into the short-ranged RB disorder⁹. Intriguingly, we observe that the current-induced DW creep belongs to a different universality class from the field-induced case. Experiments also reveal that the adiabatic STT is the dominant driving mechanism for the DW motion in this system. The obtained results indicate that the universality class for current-induced DW creep is governed by the nature of the torque and does not depend on the intricate details of the disorder.

The stack structure used for this study is, from the substrate side, Ta (0.5 nm)/CoFeB (1.2 nm)/MgO (1.5 nm)/Ta (1 nm). The ultrathin Ta underlayer reduces the current flow through it and thus suppresses the effects associated with the SOTs as compared to the STTs in current-driven DW motion, as will be shown later. Magnetization measurements on a blanket film confirm that the stack possesses an out-of-plane magnetic easy axis with a saturation magnetization M_s of 1.36 T and effective anisotropy constant K_{eff} of $2.82 \times 10^5 \text{ J m}^{-3}$. With these parameters, a DW formed in the 1.2-nm-thick CoFeB layer can be treated as a one-dimensional interface moving in the two-dimensional medium (see Supplementary Information 1). The stack is patterned into wires with width 5 μm (or 10 μm) and length 60 μm (or 120 μm), as shown in Fig. 1a. The change of DW position after the application of a magnetic field or electrical current is observed by a magneto-optical Kerr effect (MOKE) microscope. The set-up is equipped with a liquid He cryostat to change the device temperature T . Figure 1b shows typical images of domain structures after the application of current pulses with several durations at 300 K, where the differential

¹Laboratory for Nanoelectronics and Spintronics, Research Institute of Electrical Communication, Tohoku University, 2-1-1 Katahira, Aoba-ku, Sendai 980-8577, Japan. ²Center for Spintronics Integrated Systems, Tohoku University, 2-1-1 Katahira, Aoba-ku, Sendai 980-8577, Japan. ³Center for Innovative Integrated Electronic Systems, Tohoku University, 468-1 Aramaki Aza Aoba, Aoba-ku, Sendai 980-0845, Japan. ⁴WPI-Advanced Institute for Materials Research, Tohoku University, 2-1-1 Katahira, Aoba-ku, Sendai 980-8577, Japan. *e-mail: ohno@riec.tohoku.ac.jp

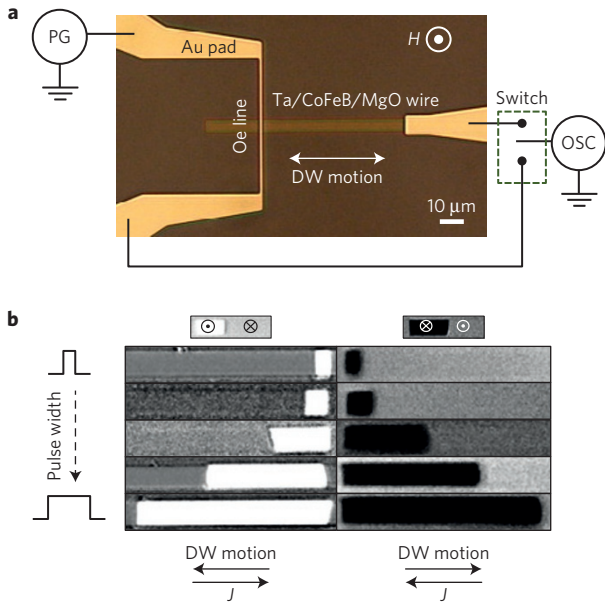


Figure 1 | Experimental set-up and MOKE images. **a**, Optical micrograph and measurement circuit. The DW is created by passing current in the Oersted (Oe) line. **b**, MOKE micrographs of DW motion under a constant current density $J = 1.5 \times 10^{11} \text{ A m}^{-2}$ with various pulse widths of 1, 2.5, 5, 7.5 and 10 ms at $T = 300 \text{ K}$. The DW has up-down (left) and down-up (right) configurations, and the black and white portions indicate the area swept by the DW. With increasing pulse width at a constant J , the displacement increases in a linear manner.

images between before and after the application of the pulse are presented; the white and black regions correspond to the areas swept by the DW. In the employed current and field range, the motion is thermally activated and is dependent on the position of the device, presumably owing to the distribution of the pinning centres. The DW displacement shows stochastic behaviour, as seen in Fig. 2a at a current density $J = 1.28 \times 10^{11} \text{ A m}^{-2}$ at $T = 300 \text{ K}$. Similar stochastic behaviour is observed also for the field-induced DW motion in the field range used in this study. We determine the DW displacement at each experimental condition by averaging the results of 50 observations. This gives us a linear dependence of DW displacement versus pulse duration, allowing us to determine the velocity from the slope of the curve. Figure 2b,c shows the displacement versus pulse duration curves obtained for a magnetic field $\mu_0 H = 0.8 \text{ mT}$ and a current density $J = 1.28 \times 10^{11} \text{ A m}^{-2}$, respectively (μ_0 is the permeability in free space).

First, we focus on the DW motion induced by the application of magnetic fields. Figure 3a shows the magnetic-field dependence of v as a function of T . The observed nonlinear dependence of $\log(v)$ on H is expected to result from the motion in the creep regime. The DW creep motion under the application of a force f ($= H$ or J) is given by the following relation^{1–10}

$$v = v_0 \exp \left[-\frac{U_c}{k_B T} \left(\frac{f_c}{f} \right)^\mu \right] \quad (1)$$

where v_0 is the velocity at threshold force $f_c = H_c$ or J_c , U_c the pinning potential, and k_B the Boltzmann constant. We fit equation (1) to the results in Fig. 3a with μ as an adjustable variable (see Supplementary Information 2 for the variation of the standard error of the fitting versus μ). The average value of μ that gives the best fit for the temperature range studied here is determined to be 0.23 ± 0.07 . Figure 3b shows $\log(v)$ versus $H^{-0.23}$, in which a linear relation between them is confirmed, proving that

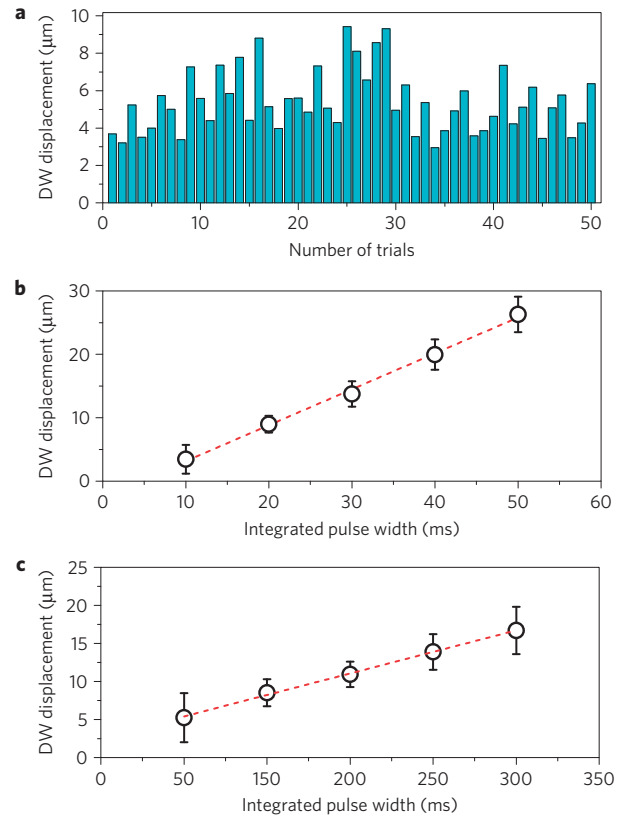


Figure 2 | Determination of DW velocity. **a**, DW displacement versus number of trials obtained at various positions along the wire for $J = 1.28 \times 10^{11} \text{ A m}^{-2}$ at $T = 300 \text{ K}$. **b**, Average displacement versus integrated pulse width under $\mu_0 H = 0.8 \text{ mT}$ at $T = 300 \text{ K}$. **c**, Average displacement versus integrated pulse width under $J = 1.28 \times 10^{11} \text{ A m}^{-2}$ at $T = 300 \text{ K}$. From the linear fit to **b** and **c** shown as broken red lines, the DW velocity is determined. Error bars denote the standard deviation calculated from 50 measurements.

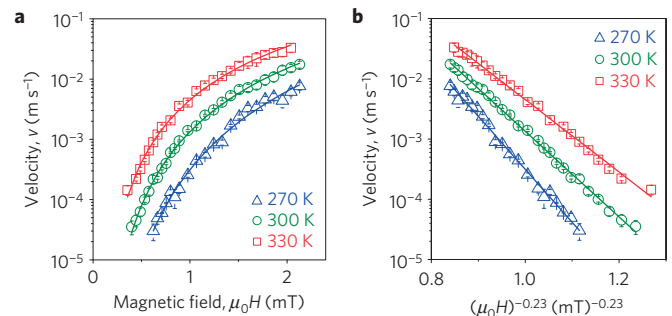


Figure 3 | Field-induced DW creep. **a**, DW velocity v versus magnetic field H for various temperatures. **b**, Scaling plot of $\log v$ versus $(\mu_0 H)^{-0.23}$. From the slope of the linear fit, we determine the effective pinning strength. Solid lines in **a** and **b** indicate the fitting curves with equation (1).

the motion is well described by equation (1). From the slope of the plot, one can determine the effective pinning strength, defined as $\mu_0 H_c^{\text{eff}} = (U_c/k_B T)^{1/\mu} \mu_0 H_c$. The magnitude of $\mu_0 H_c^{\text{eff}}$ in our system is $\sim 10^3 \text{ T}$, which is two and one orders of magnitude smaller than in the case of Co/Pt and Pt/Co₆₈B₃₂/Pt systems, respectively, with similar wire widths⁸. The weaker pinning strength may be related to the wider DW width in the CoFeB/MgO because of smaller K_{eff} .

Next we turn to the current-induced DW motion. Figure 4a shows the current-density dependence of the DW velocity at $H = 0$

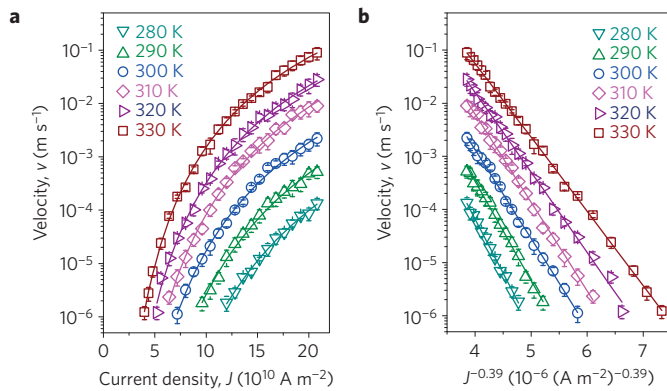


Figure 4 | Current-induced DW creep. **a**, DW velocity v versus current density J for various temperatures. **b**, Scaling plot of $\log v$ versus $J^{-0.39}$. Solid lines indicate the fitting curve with equation (1).

as a function of T . The current density in the CoFeB layer is calculated in the same way as in a previous study, taking into account bulk and surface/interface scattering of electrons²⁶; in the present case 96% of the total current flows in the CoFeB layer (see Supplementary Information 3). The motion is in the opposite sense to the current direction—that is, along the electron flow (see Fig. 1b)—as could be expected for electrons and the ferromagnetic sign of the s - d coupling. As seen in the magnetic-field case, the velocity responds nonlinearly to the applied J in the same range of v . The current-density dependence of the velocity over four orders of magnitude in Fig. 4a is again fitted by equation (1) with μ as a free variable. The result of the fit reveals that μ for current-induced creep is different from that in the field-induced case (see Supplementary Information 4). The value of μ for $300 \leq T \leq 330$ K is obtained to be 0.39 ± 0.06 . Figure 4b shows the scaling plots of the $\log(v)$ versus $J^{-0.39}$, in which the linear dependence indicates that the motion is again well described by the same equation (1), but with a different μ . The obtained value of μ seems to be incompatible with either RF or RB disorder.

Figure 5 summarizes the field- and current-induced creep exponent μ as a function of T . The field- and current-induced creep exponents are virtually independent of T , as required by the creep law. To eliminate discrepancies due to device structure or size, results from a 10- μm -wide wire are also shown for comparison (see Supplementary Information 5). It can be clearly identified that the field- and current-induced DW creeps exhibit different values of μ , hence belonging to different universality classes. This is in sharp contrast to the previous reports on metallic systems which indicate the same universality class for DW creep induced by field and current⁷. The difference of the motion induced by field and current in CoFeB/MgO thus calls for a careful consideration of the factors governing DW creep in metallic systems.

DW creep driven by magnetic field arises from the competition between the elastic energy and the range of the disorder potential. From our experimental results on the field-induced DW creep in CoFeB/MgO, we obtain $\mu = 0.23 \pm 0.07$. This is close to the theoretical value of $\mu = 0.25$ for RB disorder commonly observed in metallic systems, where the disorder potential has short-range correlations. This is in contrast to the results from the magnetic semiconductor (Ga,Mn)As (ref. 3). The difference presumably originates from the nature of the disorder potential in the magnetic semiconductor, where the pinning is believed to be due to the randomly distributed Mn moments, and thus characterized by $\mu = 1$.

The flow of current through a heavy metal (HM)/ferromagnet (FM)/oxide stack results in several different interactions. Here, because we find that both DWs with up-down and down-up configurations obey the same creep scaling relation (see

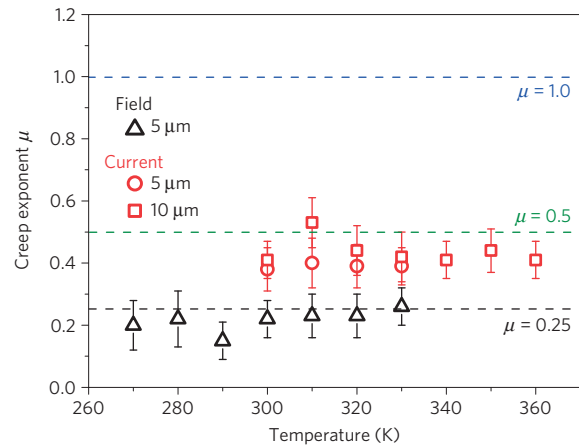


Figure 5 | Temperature dependence of creep exponents. Creep exponent μ for field- and current-driven DW creep. Broken lines show the three universality classes known at present in the literature. $\mu = 0.25$ denotes the RB disorder model, whereas $\mu = 1$ denotes the RF disorder model. $\mu = 0.5$ is the theoretical value based on the adiabatic STT model. Error bars come from the fitting error of the velocity curve shown in Figs 3a and 4a.

Supplementary Information 6), we do not take into consideration the effect of the Oersted field, and focus on the spin-related effects. First, the DW in the FM layer can be acted on by the adiabatic and/or the non-adiabatic STT from the spin-polarized current in the FM layer^{18–20}. Second, the current through the stacks with structural inversion asymmetry gives rise to the SOT (refs 21–23). Note here that the non-adiabatic torque is equivalent to the torque induced by a magnetic field along the z direction. The direction of SOT depends on the DW configuration: Bloch or Néel wall. In case of a Bloch wall, SOT has no effect on the DW, whereas for a Néel wall, the directions of anti-damping and field-like components are equivalent to the magnetic field along the z and y directions, respectively. To understand the effect of these torques on the creep, we evaluate the current-induced DW creep in the presence of an external magnetic field along the z direction (see Supplementary Information 7 and 8). We find that the critical current density and the universality class for the current-induced DW motion do not depend on a field of less than ± 0.2 mT. This indicates that the non-adiabatic STT and SOT with the anti-damping symmetry are not dominant, because the effective field due to them is estimated to be less than ± 0.06 mT. This is further supported by micromagnetic simulations and high-current flow-regime experiments, which suggest that these torques are not dominant in our system²⁴. On the other hand, the contribution of the field-like component of SOT is estimated to be less than ± 0.12 mT. As this value is much smaller than the typical magnetic-field scale of our system, and the field along the y direction cannot induce a steady DW motion, its influence is also considered not to be significant for the observed DW creep, although more rigorous investigations may be required. Thus, the adiabatic STT is likely to be the most dominant factor driving the DW and determining the universality class (see Supplementary Information 8).

A theory developed for adiabatic STT-induced DW creep is based on an assumption that the dynamics of the creep is governed by local modulation of the DW magnetization angle relating to the internal energy of the DW. Competition between the local modulation of the internal angle of the DW magnetization and the STT arising from the current in this model leads to $\mu = 0.5$ (ref. 3). In this regard, the universality class should be independent of the nature of the disorder being RB or RF. The remaining discrepancy in μ from the theoretical value of 0.5 suggests that other mechanisms/effects are also responsible for the observed exponent or the experimental results can be explained by a more rigorous theory. It can be pointed

out at this stage that a similar discrepancy was also seen in a magnetic semiconductor³.

This work sheds light on the general physics of DW creep under the action of torques with various symmetries. Our result shows that the current-induced creep belongs to a universality class that is insensitive to the nature of disorder when driven by the adiabatic STT, and suggests that it belongs to universality classes determined by the nature of disorder in the case of non-adiabatic STT or SOT. The present results thus show that DWs are expected to serve as a prototypical model of elastic systems to study the physics of creep motions under various kinds of driving forces with different symmetries.

Methods

Methods and any associated references are available in the [online version of the paper](#).

Received 21 May 2015; accepted 9 November 2015;
published online 14 December 2015

References

- Lemerle, S. *et al.* Domain wall creep in an Ising ultrathin magnetic film. *Phys. Rev. Lett.* **80**, 849–852 (1998).
- Cayssol, F., Ravelsona, D., Chappert, C., Ferre, J. & Jamet, J. P. Domain wall creep in magnetic wires. *Phys. Rev. Lett.* **92**, 107202 (2004).
- Yamanouchi, M. *et al.* Universality classes for domain wall motion in the ferromagnetic semiconductor (Ga,Mn)As. *Science* **317**, 1726–1729 (2007).
- Moore, T. A. *et al.* High domain wall velocities induced by current in ultrathin Pt/Co/AlO_x wires with perpendicular magnetic anisotropy. *Appl. Phys. Lett.* **93**, 262504 (2008).
- Kim, J., Kim, K.-J. & Choe, S.-B. Temperature dependence of domain-wall creep in Pt/CoFe/Pt films. *IEEE Trans. Mag.* **45**, 3909–3911 (2009).
- Kanda, A., Suzuki, A., Matsukura, F. & Ohno, H. Domain wall creep in (Ga,Mn)As. *Appl. Phys. Lett.* **97**, 032504 (2010).
- Lee, J.-C. *et al.* Universality classes for magnetic domain wall motion. *Phys. Rev. Lett.* **107**, 067201 (2011).
- Lavrijsen, R. *et al.* Enhanced field-driven domain-wall motion in Pt/Co₆₈B₃₂/Pt strips. *Appl. Phys. Lett.* **98**, 132502 (2011).
- Burrowes, C. *et al.* Low depinning fields in Ta–CoFeB–MgO ultrathin films with perpendicular magnetic anisotropy. *Appl. Phys. Lett.* **103**, 182401 (2013).
- Gorchon, J. *et al.* Pinning-dependent field-driven domain wall dynamics and thermal scaling in an ultrathin Pt/Co/Pt magnetic film. *Phys. Rev. Lett.* **113**, 027205 (2014).
- Blatter, G., Feigel'man, M. V., Geshkenbein, V. B., Larkin, A. I. & Vinokur, V. M. Vortices in high-temperature superconductors. *Rev. Mod. Phys.* **66**, 1125–1388 (1994).
- Buldyrev, S. V. *et al.* Anomalous interface roughening in porous media: Experiment and model. *Phys. Rev. A* **45**, R8313 (1992).
- Vicsek, T., Cserzo, M. & Horvath, V. Self-affine growth of bacterial colonies. *Physica A* **167**, 315–321 (1990).
- Chauve, P., Giamarchi, T. & Doussal, P. L. Creep and depinning in disordered media. *Phys. Rev. B* **62**, 6241–6267 (2000).
- Parkin, S. S. P., Hayashi, M. & Thomas, L. Magnetic domain-wall racetrack memory. *Science* **320**, 190–194 (2008).
- Fukami, S. *et al.* Low Current Perpendicular Domain Wall Motion Cell for Scalable High-Speed MRAM Symposium on VLSI Technology. 230–231 (IEEE, 2009).
- Burrowes, C. *et al.* Non-adiabatic spin-torques in narrow magnetic domain walls. *Nature Phys.* **6**, 17–21 (2010).
- Berger, L. Exchange interaction between ferromagnetic domain-wall and electric-current in very thin metallic-films. *J. Appl. Phys.* **55**, 1954–1956 (1984).
- Thiaville, A., Nakatani, Y., Miltat, J. & Suzuki, Y. Micromagnetic understanding of current-driven domain wall motion in patterned nanowires. *Europhys. Lett.* **69**, 990–996 (2005).
- Koyama, T. *et al.* Observation of the intrinsic pinning of a magnetic domain wall in a ferromagnetic nanowire. *Nature Mater.* **10**, 194–197 (2011).
- Emori, S. *et al.* Current-driven dynamics of chiral ferromagnetic domain walls. *Nature Mater.* **12**, 611–616 (2013).
- Torrejon, J. *et al.* Interface control of the magnetic chirality in CoFeB/MgO heterostructures with heavy metal underlayers. *Nature Commun.* **5**, 4655 (2014).
- LoConte, R. *et al.* Role of B diffusion in the interfacial Dyzaloshinskii–Moriya interaction in Ta/Co₂₀Fe₆₀B₂₀/MgO nanowires. *Phys. Rev. B* **91**, 014433 (2015).
- Fukami, S. *et al.* Current-induced domain wall motion in perpendicularly magnetized CoFeB nanowires. *Appl. Phys. Lett.* **98**, 082504 (2011).
- Ikeda, S. *et al.* A perpendicular-anisotropy CoFeB–MgO magnetic tunnel junction. *Nature Mater.* **9**, 721–724 (2010).
- Zhang, C. *et al.* Magnetotransport measurements of current induced effective fields in Ta/CoFeB/MgO. *Appl. Phys. Lett.* **103**, 262407 (2013).

Acknowledgements

We are grateful to J. Ieda, S. Barnes and T. Dietl for fruitful discussions. A portion of this work was supported by the FIRST Program of JSPS, R&D Project for ICT Key Technology to Realize Future Society of MEXT, R&D Subsidiary Program for Promotion of Academia-Industry Cooperation of METI, and ImpACT Program of CSTI. S.D. acknowledges MEXT, Govt. of Japan for financial support.

Author contributions

H.O., M.Y. and S.F. designed the experiments. S.D., C.Z. and S.F. fabricated the samples. S.D. performed measurements and data analysis. S.D. and S.F. wrote the manuscript with input from F.M. and H.O. All authors contributed to the planning and discussion of this research.

Additional information

Supplementary information is available in the [online version of the paper](#). Reprints and permissions information is available online at www.nature.com/reprints. Correspondence and requests for materials should be addressed to H.O.

Competing financial interests

The authors declare no competing financial interests.

Methods

Sample preparation. The Ta/CoFeB/MgO wires are fabricated by photolithography and Ar ion milling from a stack of Si/SiO₂ substrate/Ta(0.5 nm)/CoFeB (1.2 nm)/MgO (1.5 nm)/Ta (1 nm) deposited by d.c. and radiofrequency magnetron sputtering with Ar gas under a base pressure of less than 1×10^{-6} Pa. The Cr (5 nm)/Au (100 nm) electrodes for DW injection and contact pads are fabricated by sputtering and lift off. The devices are annealed at 300 °C for 1 h in a perpendicular magnetic field of 0.4 T.

Observation of DW motion. DW creep motion experiments are carried out in a MOKE microscope equipped with an open cycle He cryostat. An electromagnet attached to the MOKE microscope is used to apply the field pulses. The measurement procedure for the field- and current-induced DW creep motion is as follows: first the magnetization of the wire is initialized by applying an out-of-plane magnetic field. Next, a DW is created by applying a current pulse of 40 mA and duration 10 μ s to the Oersted line placed perpendicular to the magnetic wire (see Fig. 1a). Then, the created DW is moved to

the field of view of the MOKE microscope by an out-of-plane field pulse with a magnitude of 0.8–1.0 mT and duration of 10–20 ms. After that, single or multiple current or magnetic-field pulses are applied and the differential MOKE image between before and after the pulse application is recorded. The length of the displacement is calculated from the image, and a set of 50 displacements are recorded by initializing the DW at various different positions along the wire to average the effects due to extrinsic pinning sites. The pulse width is adjusted, which gives a set of measurable displacements in the MOKE microscope. The same set of experiments is repeated for different pulse widths for the same current density or magnetic field. This eliminates the transient effects due to the rise and fall time of the pulses. From the plot of the displacement versus the field or current pulse width, the DW velocity is obtained. The same set of experiments is repeated by changing the temperature of the cryostat. For the current-induced DW motion, we set the stage temperature so that the device temperature becomes constant for each applied current, where the temperature increase due to the Joule heating is taken into consideration (see Supplementary Information 9).